
Bone formation in polymeric scaffolds evaluated by proton magnetic resonance microscopy and X-ray microtomography

Newell R. Washburn,¹ Michael Weir,¹ Paul Anderson,² Kimberlee Potter^{3,4}

¹Polymers Division, National Institute of Standards and Technology, Gaithersburg, Maryland

²Centre for Oral Growth and Development, Queen Mary, University of London, London, United Kingdom

³Magnetic Resonance Microscopy Facility, Armed Forces Institute of Pathology Annex, Rockville, Maryland

⁴Section on Tissue Biophysics and Biomimetics, National Institute of Child Health and Human Development, Bethesda, Maryland.

Received 22 August 2003; revised 25 November 2003; accepted 25 February 2004

Published online 3 May 2004 in Wiley InterScience (www.interscience.wiley.com). DOI: 10.1002/jbm.a.30054

Abstract: Magnetic resonance microscopy (MRM) and X-ray microtomography (XMT) were used to investigate *de novo* bone formation in porous poly(ethyl methacrylate) (PEMA) scaffolds, prepared by a novel co-extrusion process. PEMA scaffolds were seeded with primary chick calvarial osteoblasts and cultured under static conditions for up to 8 weeks. Bone formation within porous PEMA scaffolds was confirmed by the application of histologic stains to intact PEMA disks. Disks were treated with Alizarin red to visualize calcium deposits and with Sirius red to visualize regions of collagen deposition. DNA analysis confirmed that cells reached confluence on the scaffolds after 7 weeks in static culture. The formation of bone in PEMA scaffolds was investigated with water proton MRM. Quantitative MRM maps of the magnetization transfer ratio (MTR) yielded

maps of protein deposition, and magnetic resonance (MR) relaxation times (T1 and T2) yielded maps of mineral deposition. The location of newly formed bone and local mineral concentrations were confirmed by XMT. By comparing MRM and XMT data from selected regions-of-interest in one sample, the inverse relationship between the MR relaxation times and mineral concentration was validated, and calibration curves for estimating the mineral content of cell-seeded PEMA scaffolds from quantitative MRM images were developed. © 2004 Wiley Periodicals, Inc. * J Biomed Mater Res 69A: 738–747, 2004

Key words: magnetic resonance microscopy; X-ray microtomography; tissue engineering; bone; polymer scaffold

INTRODUCTION

The limited supply of autograft material for the repair of skeletal defects has inspired an explosion of

The opinions and assertions contained herein are the private views of the authors and are not to be construed as official or reflecting the views of the Department of the Army or the Department of Defense.

Certain equipment and instruments or materials are identified in this article to adequately specify the experimental details. Such identification neither implies recommendation by the National Institute of Standards and Technology, nor that the materials are necessarily the best available for the purpose.

Published abstract appears in Proc Int Soc Magn Reson Med 2002;10:497.

Correspondence to: Kimberlee Potter, Ph.D., Department of Cellular Pathology and Genetics, Armed Forces Institute of Pathology Annex, 1413 Research Blvd., Rockville, MD 20850; e-mail: potterk@afip.osd.mil

Contract grant sponsor: NIH; contract grant number: DE14453

Contract grant sponsor: EPSRC; contract grant number: GR/R28911/01

strategies for the production of replacement bone tissue. In the majority of cases, bone cells are required to attach and grow on a three-dimensional scaffold material.¹ Two-dimensional culture techniques might be applied to three-dimensional scaffolds, but there are a number of factors that limit the success of three-dimensional cultures. To get good bone formation, there must be adequate seeding of the scaffold by the cells. This has led to a number of studies on optimal seeding techniques for porous scaffold materials.^{2–4} The success of the various seeding techniques is assessed using a DNA assay to estimate the total number of cells within the scaffold. This approach, however, yields very little information about the distribution of the cells throughout the scaffold. Other investigators have reported on the successful application of confocal microscopy to study cells growing in the pores of scaffolds,^{5,6} but the depth penetration of this technique is limited and it cannot be applied to scaffolds that are optically opaque. What is required is a nondestructive technique that can provide spatially resolved, chemically specific, tissue-level information about the bone formed within the pores of the scaffold material.

Conventional techniques, such as histomorphom-

etry, electron microscopy, and Fourier transform infrared (FT-IR) imaging, are often used in bone formation studies and are capable of giving detailed information on tissue development, but they require that scaffolds be destructively sectioned. The resulting loss of three-dimensional information is a serious limitation. Other problems include the dissolution of polymeric scaffolds by the organic solvents used in the preparation of thin sections⁷ or the disruption of early mineral deposits by aqueous solvents.⁸ A number of noninvasive optical tomography methods are available, but despite their high spatial resolution they have limited depth penetration and local area coverage, and are dependent on the use of fluorescent probes. In this work, we apply two complementary, three-dimensional microscopic techniques, magnetic resonance microscopy (MRM) and X-ray microtomography (XMT), to map the distribution of newly formed bone in novel extruded polymer scaffolds.

Magnetic resonance microscopy is a high-resolution imaging technique capable of yielding three-dimensional structural information with a resolution on the order of tens of microns. In our experiments, we monitored protons associated with water and generated maps of the magnetization transfer ratio (MTR) and magnetic resonance (MR) relaxation times T1 and T2, which provide information about protein deposition and mineral formation, respectively. Typically, proton MRM images of cortical bone yield very little signal owing to its low water content, whereas images of cancellous bone yield a bright signal owing to intervening bone marrow, which facilitates the visualization of its trabecular architecture.^{9–12} Bone can be imaged directly using solid state imaging techniques to detect the phosphorus-31 nuclei immobilized in the inorganic matrix.^{13–15} However, in a developing system the ³¹P signal from bone is not very large owing to the exceedingly small amounts of mineral deposited, which can be overwhelmed by contributions from the phosphate ions present in buffered solutions, phosphorylated cytosolic metabolites, and membrane phospholipids.¹⁶ In the proposed mineralizing system, early mineral deposits do not result in a complete loss of the water proton signal and thus proton MRM can be applied to study the distribution of bone constituents within the polymer scaffold. While MRM has been shown to yield information on the distribution of smooth muscle cells seeded onto a polylactide construct,¹⁷ quantification of the matrix produced in the scaffold would make it an even more useful tool for monitoring tissue development. To achieve this goal, we used XMT, a technique that has been shown to yield quantitative information about mineralized tissues, as a calibration tool for quantifying MRM images of identical specimens.

X-ray microtomography generates three-dimensional maps of linear absorption coefficients (LACs) based on the attenuation of X-rays.¹⁸ The mineral con-

centration in each voxel is then calculated from the known cross-sections of X-ray absorption of each element in the absorbing phase. To calculate the mineral content of newly formed bone, X-ray attenuation analysis is applied to XMT images assuming the X-ray absorption results from calcium hydroxyapatite.^{18,19} The X-ray attenuation of the organic phase of bone is low, and thus simultaneous, quantitative studies of this phase were not performed. The nondestructive analysis of engineered bone offers the distinct advantage of monitoring the time course of tissue development in porous scaffolds in three dimensions.

MATERIALS AND METHODS

Scaffold preparation

Poly(ethyl methacrylate) (PEMA) scaffolds were prepared using a co-extrusion technique described previously.²⁰ Briefly, 2.0 g of PEMA (Aldrich, Milwaukee, WI; $M_w = 100,000$ Da) and 2.0 g of poly(ethylene oxide) (PEO, Polysciences, Warrington, PA; $M_w = 100,000$ Da) were blended in a minicompounder (Daca Instruments, Goleta, CA) at 170°C for 10 min with a screw rotation rate of 50 rpm. The blend was extruded from the compounder and allowed to cool to room temperature. It was then annealed at 170°C for 45 min in a disk-shaped mold, 7 mm in diameter and 2 mm deep. Annealing has been shown to increase the domain size of the blend and can be optimized to yield blends with characteristic length scales of 100 μm .²⁰ After cooling to room temperature, the PEO was washed out of the polymer blend with distilled water. This created a continuous porous network suitable for cell seeding. These samples were labeled 50% PEMA because their void volume fraction is estimated to be about 50%.

Polymer scaffolds were rinsed with methanol, dried under vacuum, and sputter-coated with gold prior to electron microscopy. Scanning electron micrographs (SEMs) were obtained with a Jeol JL-5300 (JEOL, Inc., Peabody, MA) operating at 5 kV and 50 mA. For cell culture experiments, scaffolds were sterilized briefly with 70% ethanol and precultured in tissue culture medium for at least 2 days prior to inoculation with cells to ensure sterility.

Cell isolation

Primary osteoblasts were obtained from the third population of cells released by serial collagenase digestion of the calvarial bones of 16-day-old chick embryos.²¹ Cells were isolated with the approval and strict adherence to the guidelines of the Institutional Animal Care and Use Committee. For the final digest, minced calvaria were treated with 2 mg/mL collagenase (Roche Molecular Biochemicals, Indianapolis, IN) for 75 min at 37°C with agitation. Isolated osteoblasts were resuspended in tissue culture medium, and 2×10^6 cells were seeded onto PEMA disks (\sim diameter 7×2 mm), maintained in a 24-well plate. One hour after the

initial seeding, additional culture medium was added to the culture plate. Porous PEMA disks were maintained in static culture for up to 8 weeks in a 5% CO₂ incubator and the culture medium was changed twice a week.

Tissue culture medium was prepared by adding 50 mL of heat-inactivated fetal bovine serum (Biofluids, Rockville, MD), 5 mL of 200 mM L-glutamine (Biofluids), 0.5 mL of 250 µg/mL fungizone (Biofluids), and 0.5 mL of 10 mg/mL gentamicin reagent solution (Gibco, Gaithersburg, MD) to a 500-mL bottle of Dulbecco's Modified Eagle's Medium (Biofluids). Ascorbic acid (Sigma, St. Louis, MO) was added at each medium change, twice per week, such that its final concentration was 50 µg/mL. After one week of growth, tissue culture medium was supplemented with 1% β-glycerophosphate (Sigma). Cell-seeded PEMA constructs were removed from the culture medium, washed with phosphate buffered saline, and fixed in neutral buffered formalin at weekly intervals.

Magnetic resonance microscopy

The spatial distribution of putative mineral deposits was assessed by MRM and XMT. MRM measurements were performed on a Bruker DMX spectrometer (Bruker Biospin MRI, Inc., Billerica, MA) coupled to a wide-bore magnet operating at 9.4 T (400 MHz for ¹H). PEMA disks with and without cells were cut into strips and imaged at 37°C in tubes (o.d. 5 mm) filled with phosphate buffered saline. Typical images, acquired perpendicular to the long axis of the tube, had a field-of-view of 5 mm, a nominal in-plane resolution of 78 µm, and a 1-mm slice thickness. The following parameters were evaluated spatially for each sample, the water proton longitudinal (T1) and transverse (T2) relaxation times, the proton density (PD), and the magnetization transfer ratio (MTR).

T1 values were calculated on a pixel-by-pixel basis from 8 images acquired with a saturation recovery sequence with a range of repeat times, TR = 0.2–5 s, at a single echo time, TE = 12 ms. T2 and PD values were calculated on a pixel-by-pixel basis from 16 images acquired with a multi-echo sequence (TR = 5 s, TE = 12–192 ms). The PD values, extracted by this calculation, provide a direct measure of the number of water protons present in each pixel in the image. Assuming the PD value for saline represents 100% hydration, then the PD values for the construct, when normalized to that of saline, yield the hydration state of the tissue construct. In the absence of cells, it can yield a measure of disk porosity.

MTR maps were calculated using the following equation: $[1 - M_{so}/M_o]$, where M_{so}/M_o gives the ratio of image intensities acquired with and without the application of a 5-s, 12-µT saturation pulse, 6000 Hz off-resonance.²² This parameter provides a measure of the rate of transfer of magnetization from mobile water protons to protons on large immobile macromolecules. For collagen-containing tissues, the magnetization transfer rate is very efficient (MTR is high) and for saline it is nonexistent (MTR is zero).^{23,24}

MRM image analysis was performed using Bruker Paravision software. Unique regions-of-interest (ROIs) were identified on quantitative T1, T2, MTR, and PD maps of PEMA disks and the MRM values of the pixels within each

ROI were averaged together and reported as a mean ± standard deviation.

X-ray microtomography

To facilitate the detection of small mineral deposits, PEMA scaffolds ($n = 4$), previously subjected to MRM, were air-dried and subjected to XMT. Details about the XMT system using time-delay integration for artifact elimination are given elsewhere.²⁵ Briefly, the X-ray source in the X-TEK HMX system (X-Tek Systems, Ltd., Tring, UK) was a tungsten target operated at 60 kV and 255 mA with a 5-µm spot size. The imaging system, composed of a CsI scintillator optically coupled to a cooled CCD camera, was calibrated using a high-purity aluminum step wedge. Acquisition parameters for XMT images were typically 234 slices, with 801 projections per slice, and 600 points per projection. A standard back-projection algorithm was used to reconstruct the XMT images and the voxel size in all images was (15 µm)³. The reconstructed images were in the form of 3D arrays of linear absorption coefficients (LACs) at 40 keV. The LAC values were converted to mineral concentrations of calcium hydroxyapatite (HA) using the following relation: $LAC_{avg}/LAC_{HA} \times \rho_{HA}$, where LAC_{avg} is the average LAC for a selected region-of-interest, LAC_{HA} is the LAC of pure hydroxyapatite (3.08 cm⁻¹), and ρ_{HA} is the density of pure HA (3.18 g/cm³).¹⁹ The calculated LACs of pure H₂O, protein,¹⁹ and 50% porous PEMA at 40 keV are 0.26, 0.315, and 0.135 cm⁻¹, respectively. All XMT image analysis was performed using user-defined procedures in IDL (Interactive Data Language, Research Systems, Inc., Boulder, CO).

Histology

To verify that the tissue formed was bone, whole intact PEMA disks were treated either with Alizarin red or Sirius red for the detection of calcium (red) or collagen deposits (red), respectively.^{26,27} Bright-field images of the stained polymer disks were acquired with a light microscope to confirm the distribution of mineral deposits. Paraffin sections were not prepared because the solvents employed in the embedding process would dissolve PEMA.

DNA quantification

Cell proliferation was measured by determining the DNA content of enzymatically treated scaffolds using a PicoGreen[®] Assay (Molecular Probes, Eugene, OR) and a fluorescence microplate reader (Wallac 1420 Victor², PerkinElmer Life Sciences, Gaithersburg, MD). Scaffolds were washed twice with TE buffer (10 mM Tris-HCl, 1 mM EDTA, pH 7.5) and digested in 3 mL proteinase K solution (0.5 mg/mL proteinase K, and 0.1 mg/mL SDS in a buffered solution of 10 mM Tris-HCl and 1 mM EDTA, pH 7.5) for 14 h at 55°C with periodic shaking. After digestion, 100 µL of sample was added to 100 µL PicoGreen[®] reagent solution (diluted 200-fold with TE buffer) in a 96-well microplate, incubated for 5

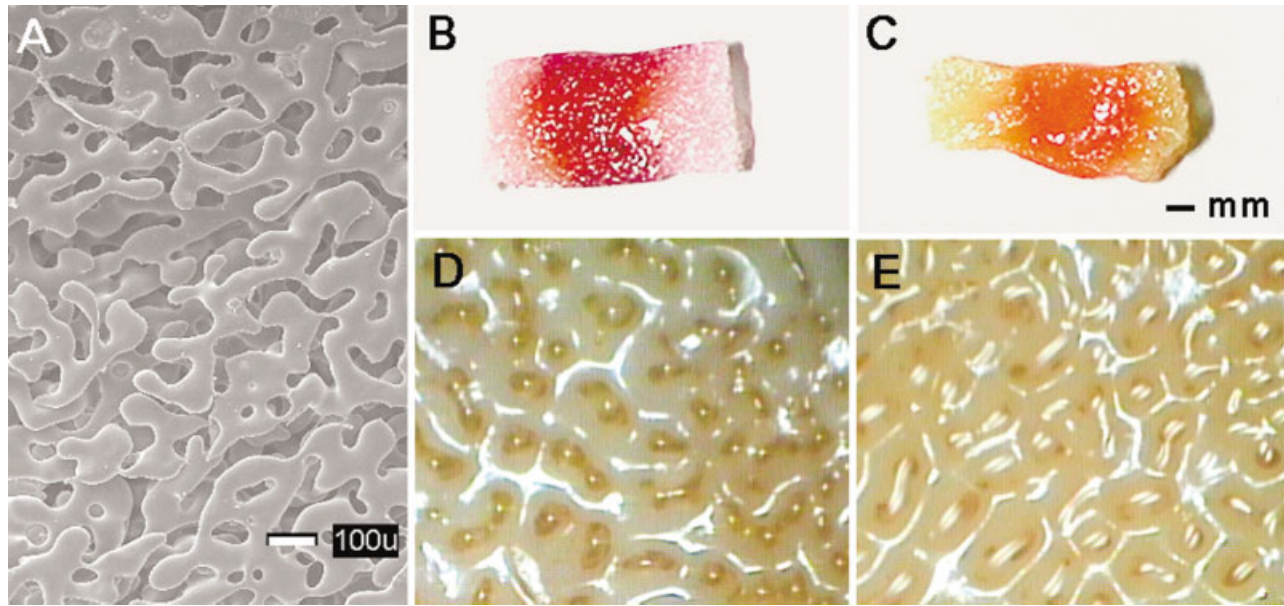


Figure 1. Scanning electron micrograph (A) of the surface of a 50% PEMA blend with a continuous void space with a characteristic length scale of 100 μm . Fragments of a cell-seeded PEMA disk maintained in culture for 5 weeks and treated with (B) Alizarin red for calcium (red) and (C) Sirius red for collagen (red). Bright-field images of the surface of the Alizarin red and Sirius red fragments are shown in (D) and (E), respectively. Stain appears to be localized in the pore spaces.

min and fluorescence emission was measured (excitation filter at 485 nm, emission filter at 535 nm). All DNA measurements were calibrated against calf thymus DNA.

RESULTS

The SEM of the surface of a typical 50% PEMA scaffold used for these studies is shown in Figure 1(A). Under the current processing conditions, the PEMA scaffold formed a continuous network of void space, with a characteristic length scale of approximately 100 μm . To confirm the formation of mineral deposits in porous PEMA disks, whole intact disks were stained with Alizarin red or Sirius red. The gross appearance of pieces cut from a cell-seeded PEMA disk, maintained in static culture for 5 weeks, and stained with Alizarin red or with Sirius red are shown in Figure 1(B,C), respectively. For the Alizarin red fragment [Fig. 1(B)], the red stain indicates the location of calcium deposits, and for the Sirius red fragment [Fig. 1(C)], the red stain indicates collagenous material. Notably, PEMA sections were not uniformly stained. Higher magnification bright-field images of the surface of sections stained with Alizarin red and Sirius red are shown in Figure 1(D,E), respectively. In both cases, the red stain was localized within the pores of the PEMA scaffold.

To assess the spatial distribution of putative mineral deposits, cell-seeded PEMA disks, maintained in static culture for 6, 7, and 8 weeks, along with unseeded PEMA scaffolds, were cut into thin rectangular strips and subjected to MRM and then XMT. Representative

MRM images of a cell-seeded PEMA disk, after 7 weeks of culture, are shown with a PEMA blank in Figure 2. Each image represents a 1-mm slice taken perpendicular to the long axis of the tube containing the two PEMA samples. The sample at the top was the cell-seeded PEMA disk and the sample at the bottom was the PEMA blank. On T2 [Fig. 2(A)], T1 [Fig. 2(B)], and PD [Fig. 2(C)] maps, areas with reduced intensity compared to the PEMA blank were attributed to areas of newly formed bone. On the MTR map [Fig. 2(D)], those same areas had high intensity values. The MTR values for the PEMA blank, however, were not measurable. According to the MRM images in Figure 2, mineral deposits were not uniformly distributed, but were restricted mostly to the cell-seeded side (or upper surface) of the PEMA disk and to crack openings, with a few deposits on the lower surface. A similar pattern of bone formation was observed for PEMA disks terminated at 6 and 8 weeks. This result suggests that under static culture conditions, cells were unable to infiltrate uniformly the PEMA scaffold.

Chemical analysis of the DNA content of PEMA disks yielded values of (117 ± 3) ng at 6 weeks, (238 ± 12) ng at 7 weeks, and (267 ± 31) ng at 8 weeks. These results suggest cell proliferation in the scaffolds had peaked after 7 weeks of culture, possibly because the cells had reached confluence in the accessible regions of the scaffold.

For the zone indicated with an arrow in Figure 2(A), T2 (39 ± 7 ms) and T1 (0.61 ± 0.16 s) relaxation times were markedly reduced compared to the PEMA blank (T2 = 86 ± 4 ms and T1 = 2.33 ± 0.14 s) and its MTR value (0.31 ± 0.09) was higher than that of the remain-

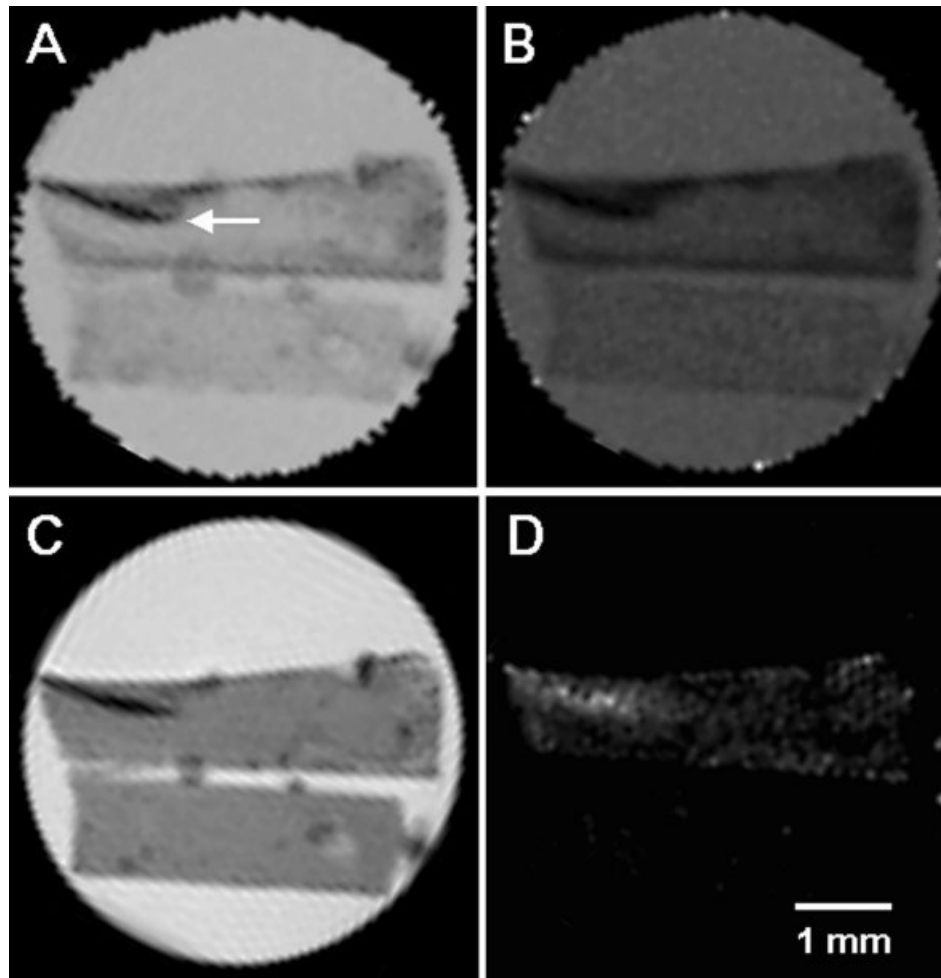


Figure 2. Quantitative T2 (A), T1 (B), PD (C), and MTR (D) maps of two PEMA specimens in a glass culture tube filled with saline. The sample at the top was a cell-seeded PEMA sample maintained in culture for 7 weeks and the white arrow indicates newly formed bone. The PEMA sample at the bottom was not seeded with cells but was included as a control for the imaging experiment. MRM images were acquired at 37°C, with an in-plane resolution of 78 μm and a slice thickness of 1 mm.

ing PEMA scaffold. Water protons in the cracks of 6- and 8-week-old samples behaved similarly, possibly because of high levels of mineral in these zones. To confirm this supposition, the 7-week-old sample in Figure 2 was air-dried and subjected to XMT.

The two-dimensional LAC images (shown in Fig. 3) were extracted from the 3D XMT data set at the approximate locations for the bottom [Fig. 3(A)], middle [Fig. 3(B)], and top [Fig. 3(C)] of the 1-mm slab of material imaged by MRM. The gray annulus observed around the PEMA samples was the glass culture tube used to contain the specimens for both MRM and XMT experiments. The PEMA scaffold appears uniformly X-ray opaque, except for those regions with mineral deposits (bright) or large air-filled pores (dark). Bright mineral deposits were colocalized with the dark zones seen on quantitative T2 and T1 maps. On close inspection, bone formation was observed to be restricted to those regions where the disk porosity was sufficient to allow for cell infiltration, specifically the upper and lower surfaces of the cell-seeded PEMA disk (at the

top) and in crack openings. The higher intensity regions observed in the PEMA blank (at the bottom) may be attributed to dystrophic mineral formed during the drying process. For comparison, 67 XMT slice images, corresponding to the 1-mm-thick slab of material imaged by MRM, were averaged in the axial direction and this averaged data set is shown in Figure 3(D).

To develop a surrogate measure for the mineral content observed in the MRM images, the X-ray derived mineral concentration map [Fig. 4(A)] calculated from Figure 3(D) was compared to the water proton T2 map [Fig. 4(B)] for the same sample. The line profiles on the right side of each image show both the mineral concentration (g/cm^3) and the T2 transverse relaxation times (ms) as a function of distance moved along the lines drawn on each image, measured from left to right. Despite the differences in image resolution, measurements made by each technique clearly correlate after suitable image registration and there is an approximate inverse

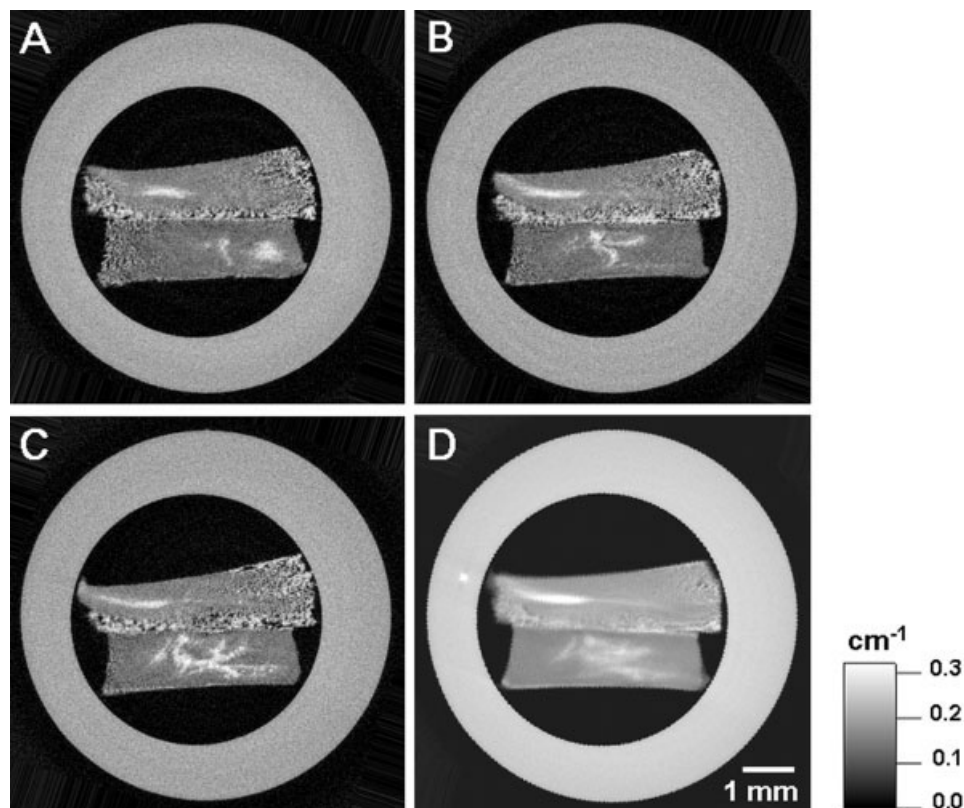


Figure 3. Two-dimensional LAC images extracted from a three-dimensional XMT data set for the same PEMA samples seen in Figure 2, after air drying. The cell-seeded PEMA disk was on top and the PEMA blank was on the bottom. Slice images shown were extracted from the approximate locations of the bottom (A), middle (B), and top (C) of the 1-mm MRM slice. A map of LAC values averaged over the 1-mm slab of material imaged by MRM is shown in (D). Regions of high intensity corresponded to mineralized areas and regions of reduced intensity were attributed to air-filled pores within the PEMA scaffold. The voxels for the XMT images were $15.221 \mu\text{m}$ on a side.

relation between mineral concentration measured by XMT and water proton T2 values measured by MRM. Thus, areas with high concentrations of mineral had low T2 values, and areas devoid of mineral had high T2 values. For the mineral concentration calculations, it was assumed that the material in the X-ray beam was composed of HA, therefore contributions from collagen molecules and the polymer scaffold were not taken into account. Accordingly, the porous PEMA scaffold was found to have the same X-ray absorption as 0.1 g/cm^3 mineral.

By comparing the mineral concentration in different regions of the cell-seeded PEMA disk with the water proton T2 and T1 relaxation times for those regions, quantitative linear relations between mineral concentration and $1/T_2$ (transverse relaxation rate) [Fig. 5(A)] and $1/T_1$ (longitudinal relaxation rate) [Fig. 5(B)] were generated. The derived linear relationships for the 7-week PEMA disk can be expressed as $1/T_2 = 0.147 [\text{HA}] - 0.004$ ($R^2 = 0.85$) and $1/T_1 = 12.37 [\text{HA}] - 0.88$ ($R^2 = 0.88$), where [HA] is the HA concentration in g/cm^3 . Both correlations were valid over the mineral concentration range found within the PEMA disks ($0.1\text{--}0.3 \text{ g/cm}^3$).

DISCUSSION

The main objective of this work was to demonstrate the use of two complementary, nondestructive imaging techniques for monitoring bone formation in polymer scaffolds produced by a co-extrusion process. To confirm that bone had formed within the polymer scaffold, various histology stains were applied to fragments of a cell-seeded PEMA disk maintained in culture for 5 weeks. Paraffin sections were not prepared because the organic solvents used for paraffin embedding would dissolve the polymer scaffold, resulting in a loss in morphological information.⁷ The red color observed for Alizarin red and Sirius red sections confirmed the deposition of mineral and collagen, respectively. The mineralized regions were not colocalized because sections represented different fragments of the same disk. The lack of red stain in other regions of the polymer confirmed the specificity of the stains for mineralized tissue. Those areas lacking mineral deposits were stained yellow from the picric acid used in conjunction with the Sirius red stain [Fig. 1(C)].

On quantitative MRM images of cell-seeded poly-

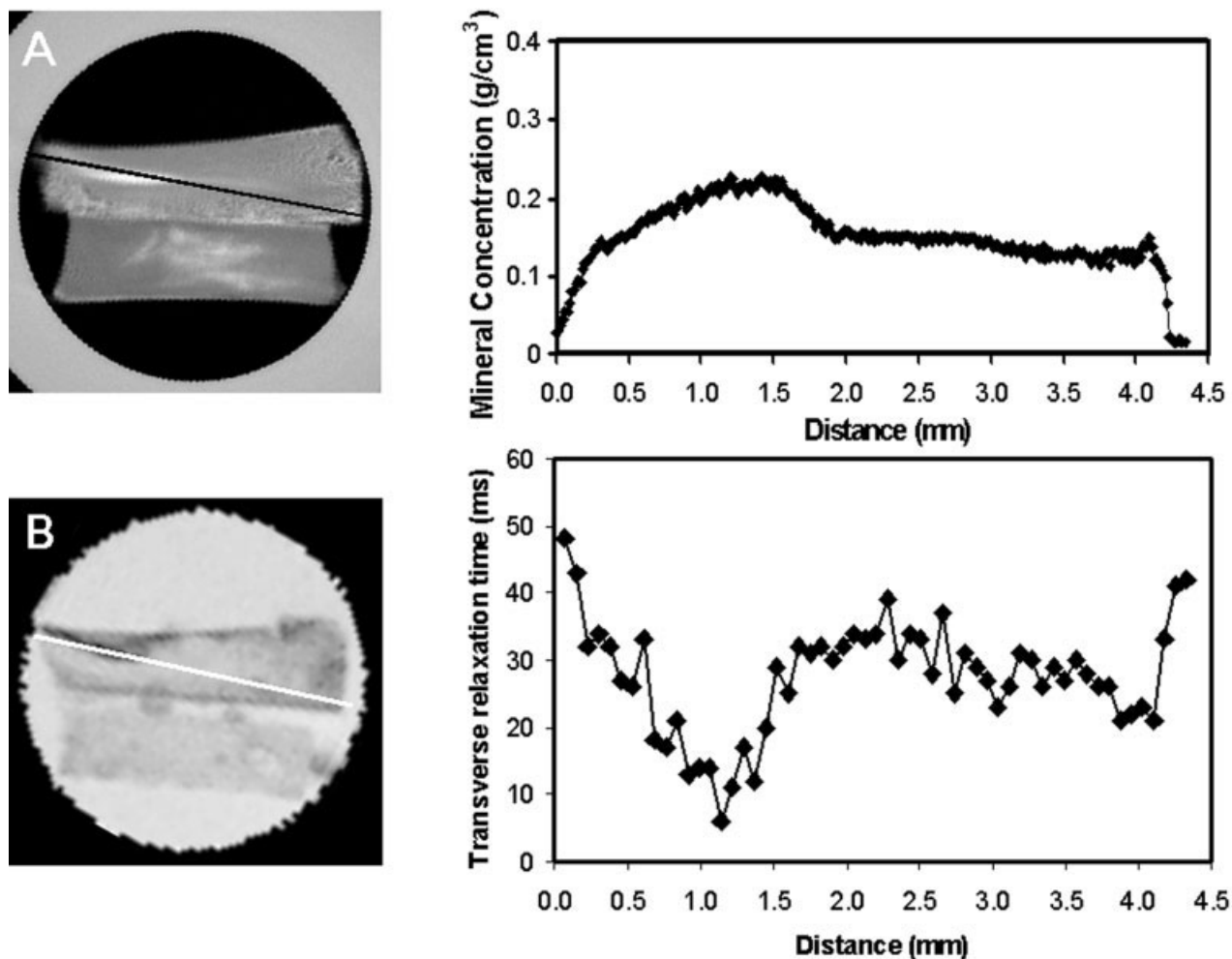


Figure 4. XMT mineral concentration map (A) calculated from the LAC map shown in Figure 3(D). This calculation assumes that the absorbing phase was pure HA and regions of high intensity corresponded to highly mineralized zones. On the corresponding T2 map (B), mineralized zones were dark. The line through each image shows the approximate location from which the XMT mineral concentration (top, right) and T2 (bottom, right) profiles were extracted.

mer disks, regions of newly formed bone [indicated with an arrow in Fig. 2(A)] had reduced water proton T1 and T2 relaxation times compared to the PEMA blank under identical imaging conditions. These results were consistent with the behavior of water proton relaxation times in the presence of *de novo* mineral deposits found in tissues undergoing endochondral ossification.^{28,29} Water proton relaxation times are highly dependent on molecular motion, thus when water molecules become immobilized through ionic or dipolar interactions at the surface of the mineral, the T1 and T2 of the surrounding solution is reduced. In the presence of mineral particles, with a different bulk magnetic susceptibility from that of water, T2 relaxation processes are further enhanced due to heterogeneities in the local magnetic field. Our results are also consistent with the findings of numerous studies aimed at understanding the effect of calcium salts on water proton MR relaxation times.^{30–33} The reduction in the image intensity of water proton density maps

can be attributed to the displacement of water by calcium salts containing no mobile protons.

For cell-seeded polymer disks, there was a measurable MT effect compared to the PEMA blank because magnetization was able to transfer between mobile water protons and macromolecular-associated protons within the newly formed bone matrix. The negligible MT effect observed for the PEMA blank confirms that this effect is solely due to newly formed bone in the PEMA scaffold. Consequently, a detectable MT effect requires the presence of specific macromolecules above a certain concentration level. For mineralized tissue formed after 7 weeks in static culture, the MTR value (0.31 ± 0.09) was higher than that reported for a cell pellet (MTR = 0.22–0.26).³⁴ Therefore, the observed MT effect cannot be attributed solely to the cell inoculum but to collagen molecules deposited in mineralized zones. This result was consistent with other reports that state that collagen has a large MT effect and it is the

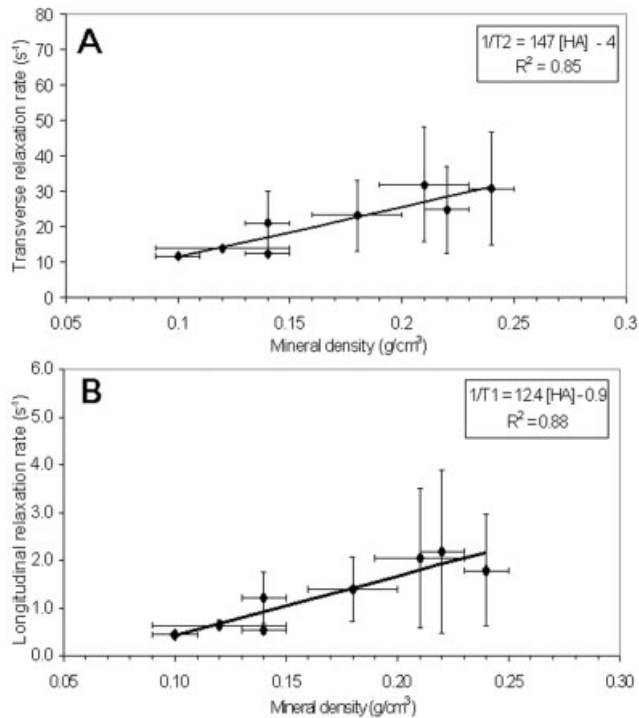


Figure 5. Calibration curves correlating mineral concentration [HA], measured by XMT, to the water proton (A) transverse ($1/T_2$) and (B) longitudinal ($1/T_1$) relaxation rates for the 7-week PEMA disk are shown. Lines were derived by regression analysis and the resulting correlations are presented in each graph.

predominant molecule that gives rise to the MT effect in collagenous tissues.^{23,35–37}

The MTR value of the highly mineralized zone [indicated with an arrow in Fig. 2(A)] was lower than MTR values reported for calcified cartilage,²⁹ and based on earlier calibration studies the measured MTR value was comparable to a 3% (w/w) collagen suspension.³⁶ A possible explanation for the low MTR value might be that the newly formed bone was very immature and not very dense, especially considering it had formed on the surface of a porous polymer scaffold. The MTR values for the superficial regions of the PEMA disk were much lower than for the highly mineralized zone, possibly because of the larger pores near the surface, which would tend to dilute the amount tissue present in the imaging voxel. This might also explain the intermediate T_1 and T_2 values observed for bone deposits near the surface. Low MTR values for regions with reduced porosity, determined from XMT images, might be attributed to a reduced number of cells that could infiltrate the space and produce large quantities of mineral and collagen. Until polymer disks can be manufactured with a uniform pore size distribution, it would be speculative to attribute the observed spatial variation in MTR values to changes in collagen content alone. Apart from changes in the collagen content, other factors could alter the measured MTR values for collagen in mineralized

zones. For example, the partial dehydration of collagen fibrils due to mineral formation in the intrafibrillar space might augment the observed MT effect. More studies, however, are required to understand how mineralization alters collagen MTR values.

Slightly brighter areas observed in XMT images of the PEMA blank were attributed to small mineral crystallites formed during the drying process, which were not present when the hydrated disk was subjected to MRM. In the XMT images presented, bone formation was restricted to those regions where the cells were able to infiltrate. Burg et al.³ demonstrated that dynamic culture conditions are necessary to promote homogeneous tissue in-growth, so it is possible that the static culture conditions used in these experiments would limit cell proliferation and mineralization to areas near the surface of the disk and in close proximity to cracks in the scaffold. The correlation of mineral concentration, as measured by XMT, with water proton relaxation rates ($1/T_2$ and $1/T_1$), as measured by MRM, were comparable to relations derived for tissue models made from agar containing a suspension of calcium hydroxyapatite in the range of 0–0.3 g/mL.³⁸

In XMT images, the polymer contributes significantly to the calculated mineral concentration. Thus, to estimate the water proton T_1 or T_2 value for water protons in a blank PEMA disk, an equivalent mineral concentration of 0.1 g/cm³ for the polymer must be substituted in the derived MRM-XMT correlations to arrive at a realistic answer. Conversely, mineral concentration calculations based on MRM measurements must be corrected for the mineral concentration contribution of the polymer. In other words, the mineral concentration will be consistently overestimated unless the mineral concentration equivalent of the polymer is taken into account. This amount is likely to be different depending on the porosity of the scaffold and, thus, the use of MRM-XMT correlations is limited to scaffolds with the same porosity and a uniform pore size distribution.

CONCLUSIONS

The formation of bone in a porous polymer scaffold was readily assessed with two noninvasive techniques, MRM and XMT. Despite the relatively low mineral densities in this system, it was possible to map mineral content with XMT and to validate the underlying relations between mineral concentration and water proton relaxation times. Through these experiments, it has been established that water proton relaxation rates can be used as surrogate measures of mineral concentration in MRM images of cell-seeded polymer scaffolds, and that this imaging modality has the added capability of being able to assess the colla-

gen present in immature bone deposits. An additional advantage of MRM over the XMT technique is that it can be used to monitor early bone formation within polymer scaffolds *in vivo* and can provide detailed information about the biological response of the body to the implanted material.³⁹

The authors are grateful to Dr. Iren Horkay (National Institute of Child Health and Human Development) for her assistance with the cell isolation procedure and Mrs. Annette Geissel, Mr. Frank Avallone, and Mr. Robert Cunningham at the Armed Forces Institute of Pathology for their histochemical expertise. This research was supported in part by NIH grant DE14453 awarded to K.P. The XMT work was supported by EPSRC grant GR/R28911/01.

References

- Crane GM, Ishaug SL, Mikos AG. Bone tissue engineering. *Nat Med* 1995;1(12):1322–13224.
- Holy CE, Shoichet MS, Davies JE. Engineering three-dimensional bone tissue *in vitro* using biodegradable scaffolds: Investigating initial cell-seeding density and culture period. *J Biomed Mater Res* 2000;51(3):376–382.
- Burg KJ, Holder WD, Jr., Culberson CR, Beiler RJ, Greene KG, Loeb sack AB, Roland WD, Eiselt P, Mooney DJ, Halberstadt CR. Comparative study of seeding methods for three-dimensional polymeric scaffolds. *J Biomed Mater Res* 2000;51(4):642–649.
- Wiedmann-Al-Ahmad M, Gutwald R, Lauer G, Hubner U, Schmelzeisen R. How to optimize seeding and culturing of human osteoblast-like cells on various biomaterials. *Biomaterials* 2002;23(16):3319–3328.
- Tjia JS, Moghe PV. Analysis of 3-D microstructure of porous poly(lactide-glycolide) matrices using confocal microscopy. *J Biomed Mater Res* 1998;43(3):291–299.
- Ishaug SL, Crane GM, Miller MJ, Yasko AW, Yaszemski MJ, Mikos AG. Bone formation by three-dimensional stromal osteoblast culture in biodegradable polymer scaffolds. *J Biomed Mater Res* 1997;36(1):17–28.
- Holy CE, Yakubovich R. Processing cell-seeded polyester scaffolds for histology. *J Biomed Mater Res* 2000;50(2):276–279.
- Pleshko NL, Boskey AL, Mendelsohn R. An FT-IR microscopic investigation of the effects of tissue preservation on bone. *Calcif Tissue Int* 1992;51(1):72–77.
- Chung HW, Wehrli FW, Williams JL, Wehrli SL. Three-dimensional nuclear magnetic resonance microimaging of trabecular bone. *J Bone Miner Res* 1995;10(10):1452–1461.
- Ouyang X, Selby K, Lang P, Engelke K, Klifa C, Fan B, Zucconi F, Hottya G, Chen M, Majumdar S, et al. High resolution magnetic resonance imaging of the calcaneus: Age-related changes in trabecular structure and comparison with dual X-ray absorptiometry measurements. *Calcif Tissue Int* 1997; 60(2):139–147.
- Majumdar S, Kothari M, Augat P, Newitt DC, Link TM, Lin JC, Lang T, Lu Y, Genant HK. High-resolution magnetic resonance imaging: three-dimensional trabecular bone architecture and biomechanical properties. *Bone* 1998;22(5):445–454.
- Majumdar S, Newitt D, Mathur A, Osman D, Gies A, Chiu E, Lotz J, Kinney J, Genant H. Magnetic resonance imaging of trabecular bone structure in the distal radius: relationship with X-ray tomographic microscopy and biomechanics. *Osteoporos Int* 1996;6(5):376–385.
- Ackerman JL, Raleigh DP, Glimcher MJ. Phosphorus-31 magnetic resonance imaging of hydroxyapatite: a model for bone imaging. *Magn Reson Med* 1992;25(1):1–11.
- Moore JR, Garrido L, Ackerman JL. Solid state phosphorus-31 magnetic resonance imaging of bone mineral. *Magn Reson Med* 1995;33(3):293–299.
- Wu Y, Ackerman JL, Chesler DA, Li J, Neer RM, Wang J, Glimcher MJ. Evaluation of bone mineral density using three-dimensional solid state phosphorus-31 NMR projection imaging. *Calcif Tissue Int* 1998;62(6):512–518.
- Brown CE, Battocletti JH, Srinivasan R, Allaway JR, Moore J, Sigmann P. *In vivo* 31P nuclear magnetic resonance spectroscopy of bone mineral for evaluation of osteoporosis. *Clin Chem* 1988;34(7):1431–1438.
- Burg KJ, Delnomdedieu M, Beiler RJ, Culberson CR, Greene KG, Halberstadt CR, Holder WD, Jr., Loeb sack AB, Roland WD, Johnson GA. Application of magnetic resonance microscopy to tissue engineering: a polylactide model. *J Biomed Mater Res* 2002;61(3):380–390.
- Wong FS, Elliott JC, Davis GR, Anderson P. X-ray microtomographic study of mineral distribution in enamel of mandibular rat incisors. *J Anat* 2000;196(Pt 3):405–413.
- Elliott JC, Wong FS, Anderson P, Davis GR, Dowker SE. Determination of mineral concentration in dental enamel from X-ray attenuation measurements. *Connect Tissue Res* 1998;38: 61–72.
- Washburn NR, Simon CG, Jr., Tona A, Elgendy HM, Karim A, Amis EJ. Co-extrusion of biocompatible polymers for scaffolds with co-continuous morphology. *J Biomed Mater Res* 2002; 60(1):20–29.
- Gerstenfeld LC, Chipman SD, Glowacki J, Lian JB. Expression of differentiated function by mineralizing cultures of chicken osteoblasts. *Dev Biol* 1987;122(1):49–60.
- Hajnal JV, Baudouin CJ, Oatridge A, Young IR, Bydder GM. Design and implementation of magnetization transfer pulse sequences for clinical use. *J Comput Assist Tomogr* 1992;16(1): 7–18.
- Kim DK, Ceckler TL, Hascall VC, Calabro A, Balaban RS. Analysis of water-macromolecule proton magnetization transfer in articular cartilage. *Magn Reson Med* 1993;29(2): 211–215.
- Ceckler TL, Wolff SD, Yip V, Simon SA, Balaban RS. Dynamic and chemical factors affecting water proton relaxation by macromolecules. *J Magn Reson* 1992;98:637–645.
- Davis GR, Elliott JC. X-ray microtomographic scanner using time-delay integration for elimination of ring artefacts in the reconstructed image. *Nucl Instrum Methods Phys Res A* 1997; 394:157–162.
- Sweat F, Puchtler H, Rosenthal SI. Sirius red F3BA as a stain for connective tissue. *Arch Pathol* 1964;78:69–72.
- Prophet EB, Mills B, Arrington JA, Sobin LH, editors. *Laboratory methods in histotechnology*. Washington DC: American Registry of Pathology; 1992. p 128–130.
- Potter K, Leapman RD, Bassar PJ, Landis WJ. Cartilage calcification studied by proton NMR microscopy. *J Bone Miner Res* 2002;17(4):652–660.
- Potter K, Landis WJ, Spencer RGS. Histomorphometry of the embryonic avian growth plate by proton nuclear magnetic resonance microscopy. *J Bone Miner Res* 2001;16(6):1092–1100.
- Davis CA, Genant HK, Dunham JS. The effects of bone on proton NMR relaxation times of surrounding liquids. *Invest Radiol* 1986;21(6):472–477.
- Tenner MS, Spiller M, Koenig SH, Valsamis MP, Childress S, Brown RD, 3rd, Kasoff SS. Calcification can shorten T2, but not T1, at magnetic resonance imaging fields. Results of a relaxation study of calcified human meningiomas. *Invest Radiol* 1995;30(6):345–353.
- Henkelman RM, Watts JF, Kucharczyk W. High signal intensity in MR images of calcified brain tissue. *Radiology* 1991; 179(1):199–206.

33. Kucharczyk W, Henkelman RM. Visibility of calcium on MR and CT: can MR show calcium that CT cannot? *AJNR Am J Neuroradiol* 1994;15(6):1145-1148.
34. Seo GS, Aoki J, Moriya H, Karakida O, Sone S, Hidaka H, Katsuyama T. Hyaline cartilage: in vivo and in vitro assessment with magnetization transfer imaging. *Radiology* 1996;201(2):525-530.
35. Wolff SD, Chesnick S, Frank JA, Lim KO, Balaban RS. Magnetization transfer contrast: MR imaging of the knee. *Radiology* 1991;179(3):623-628.
36. Gray ML, Burstein D, Lesperance LM, Gehrke L. Magnetization transfer in cartilage and its constituent macromolecules. *Magn Reson Med* 1995;34(3):319-325.
37. Potter K, Butler JJ, Adams C, Fishbein KW, McFarland EW, Horton WE, Spencer RG. Cartilage formation in a hollow fiber bioreactor studied by proton magnetic resonance microscopy. *Matrix Biol* 1998;17(7):513-523.
38. Gamsu G, de Geer G, Cann C, Muller N, Brito A. A preliminary study of MRI quantification of simulated calcified pulmonary nodules. *Invest Radiol* 1987;22(11):853-858.
39. Stroman PW, Dorvil JC, Marois Y, Poddevin N, Guidoin R. In vivo time course studies of the tissue responses to resorbable polylactic acid implants by means of MRI. *Magn Reson Med* 1999;42(1):210-214.